Chinese Chemical Letters 36 (2025) 109902

Contents lists available at ScienceDirect

Chinese Chemical Letters

journal homepage: www.elsevier.com/locate/cclet

Spatiotemporally-controlled supramolecular hybrid nanoassembly enabling ferroptosis-augmented photodynamic immunotherapy of cancer

Yuequan Wang[a], Congtian Wu[a], Chengcheng Feng[a], Qin Chen[c], Zhonggui He[a,b], Shenwu Zhang[a,b,*], Cong Luo[a,b,*], Jin Sun[a,b,*]

[a] Department of Pharmaceutics, Wuya College of Innovation, Shenyang Pharmaceutical University, Shenyang 110016, China
[b] Joint International Research Laboratory of Intelligent Drug Delivery Systems, Ministry of Education, Shenyang Pharmaceutical University, Shenyang 110016, China
[c] Department of Pharmacy, Cancer Hospital of China Medical University, Liaoning Cancer Hospital & Institute, Shenyang 110042, China

ARTICLE INFO

Article history:
Received 8 March 2024
Revised 14 April 2024
Accepted 16 April 2024
Available online 16 April 2024

Keywords:
Supermolecule
Nanoasssembly
Ferroptosis
Photodynamic therapy
Immunotherapy

ABSTRACT

Photodynamic therapy (PDT) not only directly eradicates tumor cells but also boosts immunogenicity, promoting antigen presentation and immune cell infiltration. However, the robust antioxidant defense mechanisms within tumor cells significantly weaken the efficacy of photodynamic immunotherapy. Herein, a supramolecular hybrid nanoassembly is constructed by exploring the synergistic effects of the photodynamic photosensitizer (pyropheophorbide a, PPa) and the ferroptosis inducer (erastin). The erastin-mediated inhibition of system X_c^- significantly downregulates glutathione (GSH) expression, amplifying intracellular oxidative stress, leading to pronounced cell apoptosis, and promoting the release of damage-associated molecular patterns (DAMPs). Additionally, the precise cooperation of PPa and erastin enhances ferroptosis efficiency, exacerbating the accumulation of lipid peroxides (LPOs). Ultimately, LPOs serve as a "find me" signal, while DMAPs act as an "eat me" signal, collectively promoting dendritic cell maturation, enhancing infiltration of the cytotoxic T lymphocytes, and eliciting a robust immune response. This study opens new horizons for enhancing tumor immunotherapy through simultaneous ferroptosis-PDT.

Immunotherapy has emerged as a revolutionary approach in cancer treatment, demonstrating immense potential in harnessing the body's immune system to combat tumors [1]. While immunotherapy holds promise in eliminating existing tumors and preventing tumor recurrence, it is important to note that the current immunotherapeutic approaches prove beneficial only for a specific group of cancer patients [2,3]. This limitation stems from the fact that tumor cells typically exhibit low immunogenicity, evading detection by immune cells such as dendritic cells (DCs) and T lymphocytes. Consequently, eliciting an effective antitumor immune response at the tumor site remains a significant obstacle.

Some cancer therapies, including chemotherapy, photodynamic therapy (PDT), and radiotherapy, not only eliminate tumor cells but also trigger robust immune responses [3–5]. PDT, with its exceptional tumor selectivity, noninvasiveness, and minimal systemic toxicity, is particularly notable in tumor therapy [6]. Under laser radiation, the excited photosensitizer transfers its energy to molecular oxygen, leading to the generation of reactive oxygen species (ROS) [7–10]. These ROS initiate damage to crucial intracellular targets at both organelle and molecular levels. This process not only directly eradicates tumor cells but also stimulates the release of damage-associated molecular patterns (DAMPs), such as calreticulin (CRT), high mobility group protein B1 (HMGB1), and adenosine triphosphate (ATP) [11,12]. Furthermore, DAMPs promote the maturation of DCs, facilitate antigen presentation, and trigger an anti-tumor immune response. However, in response to ROS-induced intracellular photodamage, the essential intracellular antioxidant, glutathione (GSH), counteracts oxidative stress in an effort to maintain redox homeostasis [13,14]. This defensive mechanism weakens the efficacy of PDT.

Numerous literature studies emphasize the crucial role of GSH in maintaining intracellular redox homeostasis. Certain ferroptosis inducers, such as erastin (Era), operate by inhibiting system X_c^-, resulting in the downregulation of GSH expression [15]. This disruption of the intracellular antioxidant system interferes with the

* Corresponding authors.
E-mail addresses: zhangshenwu@aliyun.com (S. Zhang), luocong@syphu.edu.cn (C. Luo), sunjin@syphu.edu.cn (J. Sun).

https://doi.org/10.1016/j.cclet.2024.109902
1001-8417/

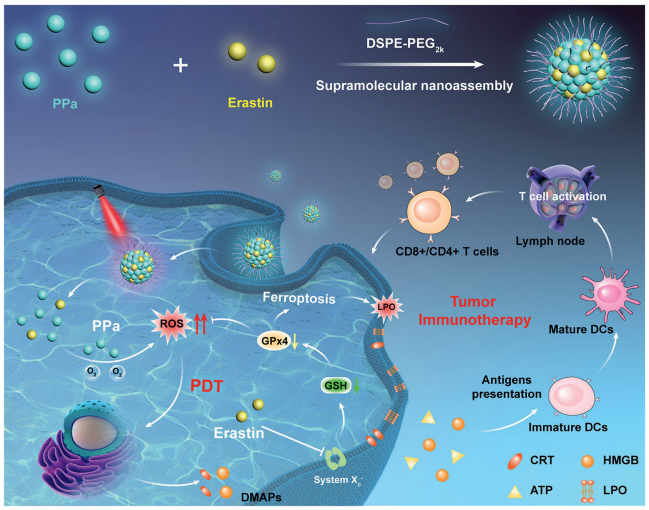

Fig. 1. Schematic representation of spatiotemporally-controlled supramolecular hybrid nanoassemblies (PPa@Era NAs) enabling ferroptosis-augmented photodynamic immunotherapy of cancer.

redox balance and exhibits a synergistic effect with PDT [16]. Additionally, the significant production of ROS during photodynamic processes, along with the disruption of the intracellular antioxidant system, leads to the accumulation of lipid peroxides (LPOs), intensifying ferroptosis [17]. Notably, LPOs can also serve as a "find me" signal, promoting antigen presentation and triggering immune response. Ultimately, the released DAMPs triggered by PDT and the accumulation of LPOs resulting from ferroptosis work together to promote an anti-tumor immune response [18].

Given the promising synergies between ferroptosis inducers and photodynamic therapy, along with their collaborative role in enhancing immune activation, a precise combination of these agents could significantly improve cancer treatment efficiency. However, simultaneous delivery of two drugs remains challenging. Nanomedicine engineering offers a solution to this obstacle. Through rational design of nanodrug delivery systems (nano-DDS), we can enhance drug physicochemical properties and improve *in vivo* delivery efficiency. Particularly, the emergence of carrier-free nanoassemblies formed by drugs themselves presents a promising nanoplatform for efficient drug delivery, boasting advantages such as high drug loading efficiency, flexible drug proportions adjustment, simple preparation process, and minimal carrier-related side effects. Herein, we have constructed supramolecular hybrid nanoassemblies co-assembled with the photodynamic photosensitizer pyropheophorbide a (PPa) and the ferroptosis inducer Era (Fig. 1). Initially, the most effective synergistic dose ratio of PPa and Era was assessed in 4T1 cells across various molar ratios. As shown in Fig. S1 and Table S1 (Supporting information), the results revealed that the combination solution of PPa and Era at a molar ratio of 3:1 (PPa/Era) demonstrated the highest cytotoxicity, showing a considerable synergistic effect with combination index (CI) values reaching 0.49. Then, according to the optimal synergy dose ratio of 3:1 (PPa/Era), the non-PEGylated supramolecular hybrid nanoassemblies (non-PPa@Era NAs) were fabricated using carrier-free nanoassembly technology [19,20]. As shown in Fig. S2 (Supporting information), the mean particle size of non-PPa@Era NAs was approximately 95 nm, indicating good nanoassembly capability. To enhance the stability and prolong the blood circulation time of the nanoassemblies, the amphiphilic modifier (1,2-distearoyl-*sn*–glycero-3-phosphoethanolamine-*N*-[amino(polyethylene glycol)–2000, DSPE-PEG_{2k}) was introduced to prepared PEGylated supramolecular hybrid nanoassemblies (PPa@Era NAs) following our previous works (Fig. 2A) [21,22]. As depicted in Fig. 2B and Table S2 (Supporting information), the mean diameter of PPa@Era NAs slightly increased to around 120 nm, and its zeta potential reduced from approximately –12 mV to –24 mV, contributing to improved colloidal stability. As anticipated, PEGylated decoration significantly enhanced the stability of PPa@Era NAs. As shown in Fig. 2C, it is evident that the particle size of PPa@Era NAs remained relatively unchanged during incubation with PBS supplemented with 10% fetal bovine serum (FBS) for 24 h. Moreover, transmission electron microscopy (TEM) revealed the uniform sphericity of PPa@Era NAs.

The remarkable nanoassembly capability observed between PPa and Era motivated a comprehensive investigation into their assembly mechanism. To delve into the intermolecular interactions between PPa and Era, molecular docking simulations were employed. As depicted in Figs. 2D and E, two predominant intermolecular forces were identified as the driving factors behind the co-assembly of PPa and Era, including hydrophobic interaction and π-π stacking interaction. Subsequently, the interaction forces between PPa and Era were confirmed by incubating the nanoassemblies with three commonly used intermolecular interaction disruptors (sodium dodecyl sulfate (SDS), KCl and urea). As shown in Fig. 2F, the particle sizes of both PPa@Era NAs distinctly increased in the presence of SDS, revealing the pivotal role of hydrophobic interaction in the nanoassembly process. In contrast, no noticeable change in particle size was observed when incubated with KCl or urea, aligning with the molecular simulation results. Furthermore, obvious redshift in the ultraviolet (UV) absorbance spectra of PPa@Era NAs was noted compared to free PPa solution (Fig. 2G), indicating the presence of π-π stacking interaction in the supramolecular hybrid nanoassemblies. As illustrated in Fig. 2H, the fluorescence intensity of PPa significantly decreased after co-assembly with Era, attributed to the aggregation caused quench (ACQ) effect of PPa in the aggregated state.

The excellent assembly capability and colloidal stability of PPa@Era NAs motivated further exploration of their therapeutic advantages at the cellular level. Firstly, the cellular uptake of hybrid nanoassemblies was observed through confocal microscopy and quantitatively determined *via* flow cytometry. As shown in Figs. 3A–C, PPa sol and PPa@Era NAs were internalized into tumor cells in a time-dependent manner. Remarkably, PPa@Era NAs demonstrated significantly higher cellular uptake efficiency than PPa sol under identical conditions. This difference may arise from the distinct uptake mechanisms of free drugs and nanomedicines. Most free drug molecules enter cells through a concentration-dependent passive diffusion, whereas nanomedicines can be efficiently internalized through concentration-independent endocytosis pathways [23–26]. Enhanced cellular uptake undoubtedly augments photodynamic cytotoxicity. Next, we investigated the cellular ROS generation ability of hybrid nanoassemblies in 4T1 cells. As depicted in Fig. S4 (Supporting information), cells treated with PPa@Era NAs exhibited much stronger fluorescence signals under laser irradiation compared to PPa sol, suggesting the excellent cellular ROS generation ability of nanoassemblies under laser irradiation, likely attributed to efficient cellular uptake. The favorable cellular uptake and ROS generation of hybrid nanoassemblies prompted a deeper exploration of synergistic cytotoxicity. As shown in Fig. 3D and Table S4 (Supporting information), the PPa@Era NAs + Laser group demonstrated the highest cytotoxicity against 4T1 cells compared to the other groups, indicating significant advantages in the synergistic and synchronous delivery of PPa and Era. Furthermore, the observed synergistic cytotoxicity was also demonstrated in CT26 cells (Fig. 3E). Subsequently, cellular apoptosis after treatment with different formulations was detected using flow cytometry with Alexa Fluor 488 Annexin V/propidium iodide (PI) dual staining kits. Consistent with the cytotoxicity results, a substantial proportion of

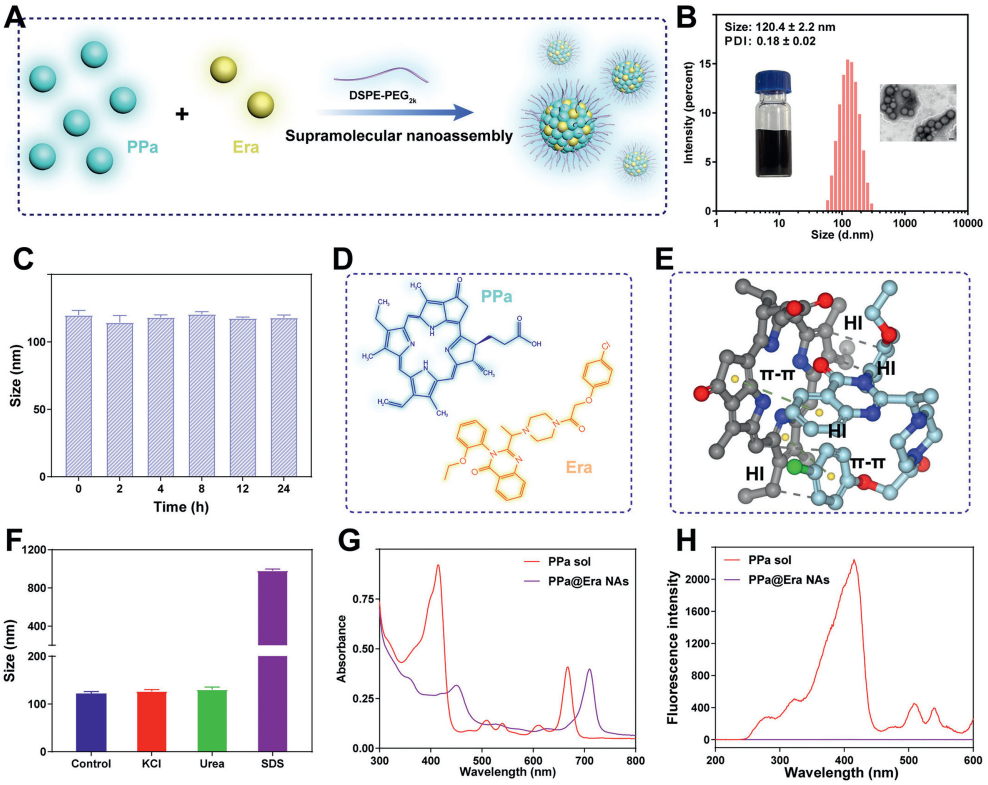

Fig. 2. The characterization of PPa@Era NAs. (A) Schematic representation of the nanoassembly process of PPa@Era NAs. (B) Appearance photos, TEM images and particle size distribution profiles of PPa@Era NAs. Scale bar: 100 μm. (C) The colloidal stability of PPa@Era NAs after incubation in PBS containing 10% FBS for 24 h at 37 °C. (D) The chemical structure of PPa and Era. (E) Molecular docking simulation depicting the intermolecular interactions between PPa and Era. π-π: π-π stacking interaction. HI: hydrophobic interaction. (F) Diameter changes of PPa@Era NAs in the presence of KCl, urea and SDS, respectively. (G) UV absorption spectra of PPa solution (sol) and PPa@Era NAs. (H) Fluorescence spectra of PPa sol and PPa@Era NAs spanning from 250 nm to 600 nm. Data are presented as mean ± standard deviation (SD) ($n = 3$).

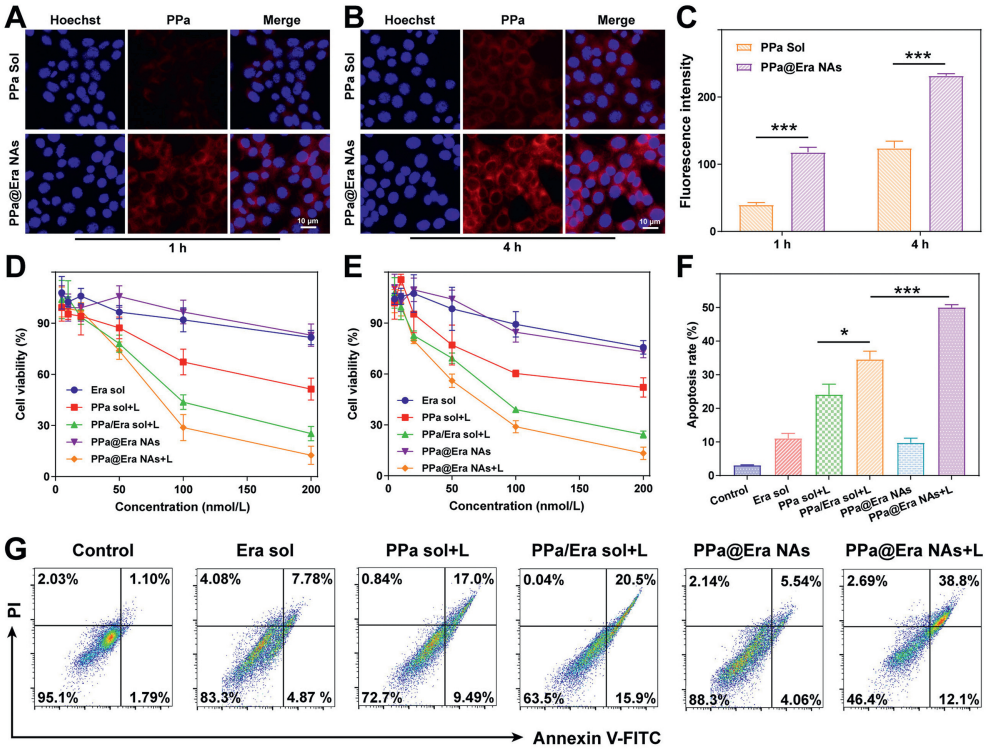

Fig. 3. Cellular uptake and *in vitro* antitumor effect of supramolecular hybrid nanoassemblies. (A, B) Cellular uptake of 4T1 cells by confocal microscopy at 1 and 4 h. Scale bar: 10 μm. (C) Quantitative analysis of cellular fluorescence intensity by flow cytometry. (D) Synergistic cytotoxicity of various formulations against 4T1 cells with/without laser irradiation (660 nm, 50 mW/cm^2, 5 min). (E) Synergistic cytotoxicity of various formulations against CT26 cells with/without laser irradiation (660 nm, 50 mW/cm^2, 5 min). (F, G) Annexin V/PI analysis of 4T1 cells incubated with different formulations, with or without 660 nm laser irradiation (660 nm, 50 mW/cm^2, 5 min). $^*P < 0.05$, $^{***}P < 0.001$. Data are presented as mean ± SD ($n = 3$).

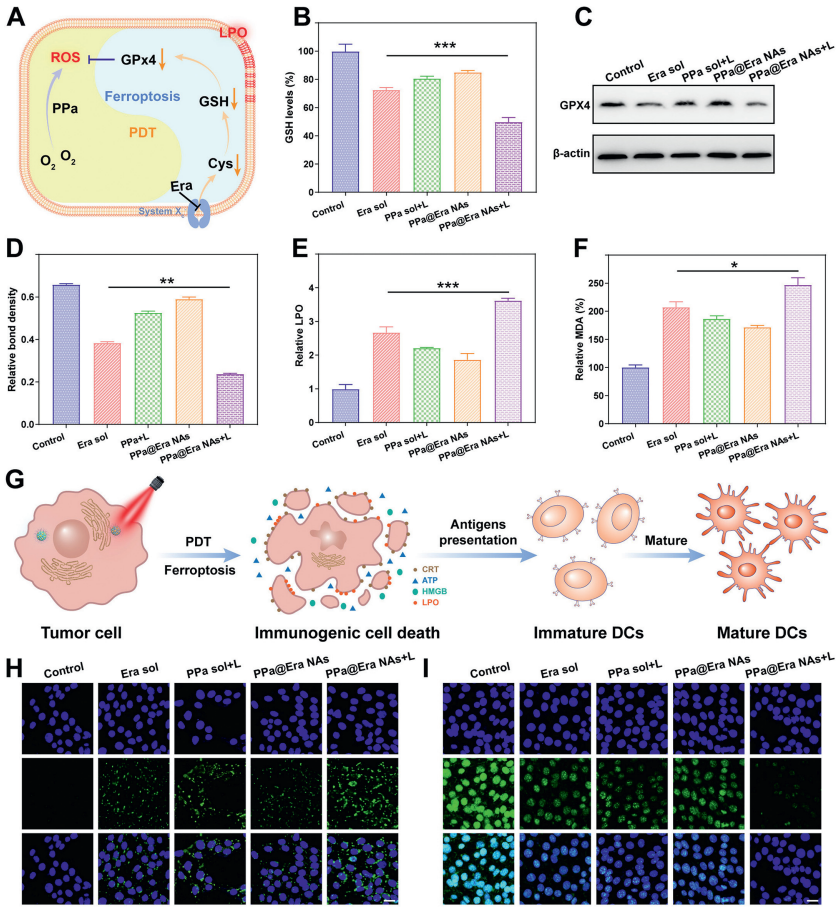

Fig. 4. Synergistic mechanism of inducing ferroptosis and ICD. (A) Schematic illustration of the synergistic enhancement of intracellular oxidative stress by PPa and Era. (B) Intracellular GSH levels in 4T1 cells after treatments. (C, D) WB analysis results of intracellular GPX4 in 4T1 cells after treatments. (E) LPOs levels in 4T1 cells after treatments. (F) MDA levels in 4T1 cells after treatments. (G) Schematic illustration of inducing ICD. (H) Confocal laser scanning microscope (CLSM) images of CRT exposure in 4T1 cells. (I) CLSM images of HMGB1 release in 4T1 cells. Scale bar: 100 μm. $^{*}P < 0.05$, $^{**}P < 0.05$, $^{***}P < 0.001$. Data are presented as mean ± SD ($n = 3$).

cell apoptosis (>50%) was observed upon exposure to PPa@Era NAs under laser irradiation (Figs. 3F and G).

Given the potent cytotoxicity of PPa@Era NAs, we explored the synergistic mechanisms between PPa and Era. System X_c^- serves as a reverse transporter responsible for importing cystine into cells, crucial for GSH synthesis. Era, a ferroptosis inducer, inhibits system X_c^-, depleting GSH and ultimately inactivating glutathione peroxidase 4 (GPX4) [26,27]. In addition, PDT-generated ROS can also consume GSH (Fig. 4A). Following this, intracellular GSH levels were quantitatively assessed using the GSH content assay kit post-treatments. As shown in Fig. 4B, GSH levels in 4T1 cells treated with various formulations (Era sol, PPa sol + Laser, PPa@Era NAs, and PPa@Era NAs + Laser) decreased to a certain extent compared to the control group. Particularly noteworthy was the PPa@Era NAs + Laser group, exhibiting the most significant GSH depletion, attributed to the effective synergistic action of PDT and the ferroptosis inducer. Additionally, intracellular GPX4 content was quantitatively assessed through Western blot (WB) post-treatments. As depicted in Figs. 4C and D, the PPa@Era NAs + Laser group also demonstrated the most robust down-regulation of GPX4. In the end, the combination of substantial ROS generated by PDT, GSH depletion and GPX4 downregulation resulted in severe lipid peroxidation. Hence, we investigated intracellular LPOs production using the C11-BODIPY 581/591 probe and quantified malondialdehyde (MDA), a LPOs product, with MDA content assay kit. As expected, the PPa@Era NAs + Laser group induced the highest intracellular accumulation of LPOs and MDA (Figs. 4E and F), aligning with the cytotoxicity results.

Substantial evidence indicates that the heightened oxidative stress resulting from the accumulation of ROS can effectively trigger immunogenic cell death (ICD) in tumor cells. This process involves the generation of DAMPs, including the exposure of CRT on tumor cells, release of HMGB1, and secretion of ATP (Fig. 4G). Consequently, we examined the alterations in typical DAMPs (CRT, HMGB1, and ATP) in 4T1 cells. As illustrated in Figs. 4H and I and Figs. S5–S7 (Supporting information), all treated groups exhibited a certain degree of DAMPs release, attributed to intracellular oxidative stress. Remarkably, PPa@Era NAs significantly elevated CRT exposure, HMGB1 release, and ATP secretion under laser irradiation. This enhancement could be attributed to the synergistically heightened levels of oxidative stress induced by the combination of PPa and Era.

The excellent *in vitro* therapeutic effectiveness of supramolecular hybrid nanoassemblies prompted us to delve into their *in vivo* delivery efficiency and tumor-specific accumulation capacity. All animal experiments were conducted with the approval of the Animal Ethics Committee of Shenyang Pharmaceutical University. The pharmacokinetic profiles of the nanoassemblies were assessed by quantitatively measuring PPa levels in plasma at various time intervals following intravenous injection in Sprague Dawley rats. As depicted in Fig. S8 and Table S5 (Supporting information), PPa sol exhibited rapid clearance from the bloodstream. In contrast, PPa@Era NAs demonstrated a prolonged circulation time in the blood and a higher area under the concentration–time curve (AUC) compared to PPa sol at an equivalent PPa dosage. These findings could be attributed to the good assembly capability, ex-

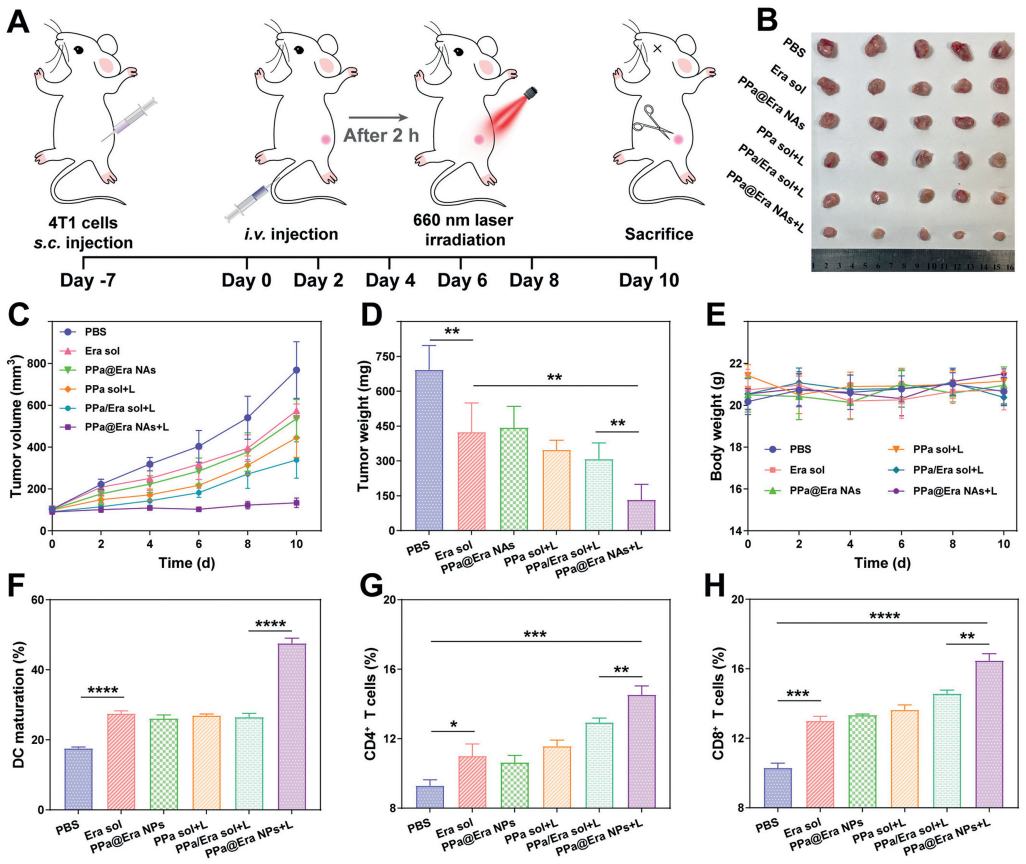

Fig. 5. *In vivo* ferroptosis-augmented photodynamic immunotherapy. (A) Schematic depiction of the experimental approach for the evaluation of the anti-tumor efficacy. (B) Tumors image of 4T1 breast tumor. (C) Tumor growth profiles ($n = 5$). (D) Tumor burden ($n = 5$). (E) Body weight changes of 4T1 breast tumor-bearing BALB/c mice ($n = 5$). (F) DCs maturation ratio in the tumor-draining lymph nodes ($n = 3$). (G) The percentage of tumor-infiltrating $CD4^+$ T cells ($n = 3$). (H) The percentage of tumor-infiltrating $CD8^+$ T cells ($n = 3$). $^*P < 0.05$, $^{**}P < 0.05$, $^{***}P < 0.001$, $^{****}P < 0.0001$. Data are presented as mean ± SD.

cellent colloidal stability, and the hydrophilic surface conferred by PEGylated modification. The prolonged blood circulation of the nanoassemblies undoubtedly facilitates tumor-specific accumulation through the enhanced permeability and retention (EPR) effect. Therefore, the tumor accumulation of nanoassemblies was conducted in 4T1-bearing BALB/c mice using *In vivo* imaging systems (IVIS). As shown in Figs. S9 and S10 (Supporting information), both the PPa@Era NAs and PPa sol groups exhibited the highest tumor accumulation at 2 h. Significantly, PPa@Era NAs displayed much higher tumor accumulation compared to PPa sol, which should be attributed to the prolonged circulation time in the blood (Figs. S9 and S10).

Additionally, we established a 4T1 breast tumor-bearing mouse model to investigate the antitumor response of PPa@Era NAs (Fig. 5A). As depicted in Figs. 5B–D, the sol group (Era sol, PPa sol + Laser, and PPa/Era sol + Laser) exhibited only moderate tumor inhibitory effects, attributed to their rapid blood clearance and inadequate tumor accumulation (Figs. S8–S10). Notably, PPa@Era NAs significantly eradicated tumors under laser irradiation, showcasing a clear advantage over other formulations (Figs. 5B–D). Hematoxylin and eosin (H&E) staining conducted on tumor sites revealed extensive apoptosis and necrosis in 4T1 breast tumors upon treatment with PPa@Era NAs under laser irradiation (Fig. S11 in Supporting information). The potent therapeutic efficacy of PPa@Era NAs can be attributed to its excellent assembly capacity (Figs. 2A and B), favorable colloidal stability (Fig. 2C), efficient cellular uptake (Figs. 3A–C), synergistic cytotoxicity (Figs. 3D and E), satisfactory pharmacokinetics (Fig. S8), and tumor-specific accumulation (Figs. S9 and S10). Moreover, no significant alterations were observed in the body weight and hematological parameters of 4T1 breast tumor-bearing mice post-treatment (Fig. 5E and Fig. S12 in Supporting information). Furthermore, major organs (heart, liver, spleen, lung, and kidney) displayed no noticeable histological changes (Fig. S13 in Supporting information).

It has been established that LPOs instigated by ferroptosis function as a "find me" signal. Concurrently, DMAPs serve as an "eat me" signal. Together, these signals collectively contribute to the maturation of DCs, augmenting the infiltration of cytotoxic T lymphocytes and fostering a robust immune response. Consequently, we proceeded to investigate the induction of DCs maturation *in vivo*. As illustrated in Fig. 5F and Fig. S13, PPa@Era NAs exhibited a significant advantage over other formulations. Impressively, PPa@Era NAs induced approximately a 2.7-fold increase in DCs maturation under laser irradiation compared to the phosphate buffer solution (PBS) control. Matured DCs play a crucial role in presenting antigens to naive T lymphocytes, thereby promoting T cell proliferation. To evaluate the potency and contribution of immune-mediated antitumor activity, the infiltration of immune cells ($CD8^+$ T cells and $CD4^+$ T cells) into the tumors was assessed, as an increase in $CD8^+$ T and $CD4^+$ T cell population signifies a robust immune response. As depicted in Figs. 5G and H and Figs. S14 and S15 (Supporting information), the tumor infiltration of both $CD8^+$ T cells and $CD4^+$ T cells experienced a substantial increase after treatment with PPa@Era NAs under laser irradiation compared to other formulations. Furthermore, the levels of several pivotal cytokines were analyzed using ELISA kits. As shown in Figs. S16 and S17 (Supporting information), PPa@Era NAs induced an up-regulation of tumor necrosis factor alpha (TNF-α)

and interferon gamma (IFN-γ) under laser irradiation. Taken together, these results suggested that PPa@Era NAs triggered a powerful anti-tumor immune response.

In summary, we developed a supramolecular hybrid nanoassemblies (PPa@Era NAs) inspired by the synergistic effect of ferroptosis and PDT. *In vitro*, PPa@Era NAs exhibited favorable colloidal stability, efficient cellular uptake, synergistic cytotoxicity, ICD induction, and LPOs accumulation. *In vivo*, they displayed satisfactory pharmacokinetics, tumor-specific accumulation, triggered a potent anti-tumor immune response, ultimately leading to successful tumor eradication.

Declaration of competing interest

The authors declare that they have no known competing financial interests or personal relationships that could have appeared to influence the work reported in this paper.

CRediT authorship contribution statement

Yuequan Wang: Writing – original draft, Methodology, Investigation. **Congtian Wu:** Software, Methodology, Investigation. **Chengcheng Feng:** Validation, Software, Resources. **Qin Chen:** Validation, Supervision, Project administration. **Zhonggui He:** Writing – review & editing, Validation, Supervision. **Shenwu Zhang:** Writing – review & editing, Validation, Conceptualization. **Cong Luo:** Writing – review & editing, Resources, Project administration, Funding acquisition. **Jin Sun:** Writing – review & editing, Validation, Supervision, Resources, Project administration, Conceptualization.

Acknowledgments

This work was financially supported by the National Natural Science Foundation of China (No. 82161138029), the Basic Research Projects of Liaoning Provincial Department of Education (No. LJKZZ20220109), and the Shenyang Youth Science and Technology Innovation Talents Program (No. RC210452).

Supplementary materials

Supplementary material associated with this article can be found, in the online version, at doi:10.1016/j.cclet.2024.109902.

References

[1] Z. Li, X. Lai, S. Fu, et al., Adv. Sci. 9 (2022) 2201734.
[2] C. Wang, H. Yu, X. Yang, et al., Asian J. Pharm. Sci. 17 (2022) 412–424.
[3] H. Chen, J. Song, Y. Wang, et al., Chem. Eng. J. 481 (2024) 148268.
[4] S. Zhang, J. Wang, Z. Kong, et al., Biomaterials 282 (2022) 121433.
[5] X. Liu, Y. Liu, X. Li, et al., ACS Nano 16 (2022) 9240–9253.
[6] F. Yang, Q. Ji, R. Liao, et al., Chin. Chem. Lett. 33 (2022) 1927–1932.
[7] Z. Shi, Q. Li, L. Mei, Chin. Chem. Lett. 31 (2020) 1345–1356.
[8] M. Zhang, Y. Zhao, H. Ma, et al., Theranostics 12 (2022) 4629–4655.
[9] Y. Wang, C. Luo, S. Zhou, et al., Asian J. Pharm. Sci. 16 (2021) 643–652.
[10] D. Wang, W. Ma, Y. Huang, et al., Chem. Eng. J. 468 (2023) 143731.
[11] C. Luo, B. Sun, C. Wang, et al., J. Control. Release 302 (2019) 79–89.
[12] M. Warszyńska, P. Repetowski, J.M. Dąbrowski, Coord. Chem. Rev. 495 (2023) 215350.
[13] Z. Lin, Y. Wang, W. Li, et al., Asian J. Pharm. Sci. 19 (2024) 100892.
[14] B. Ji, M. Wei, B. Yang, Theranostics 12 (2022) 434–458.
[15] R. Liu, C. Luo, Z. Pang, et al., Chin. Chem. Lett. 34 (2023) 107518.
[16] J. Lou, M. Aragaki, N. Bernards, et al., Biomaterials 292 (2023) 121918.
[17] Q. Chen, G. Liu, S. Liu, et al., Trends Pharmacol. Sci. 39 (2018) 59–74.
[18] S. Tao, Y. Song, S. Ding, et al., Carbohyd. Polym. 317 (2023) 121089.
[19] Y. Liu, H. Wu, S. Wang, et al., Mater Today 68 (2023) 125–147.
[20] Z. Wang, S. Zhang, Z. Kong, et al., Cell Rep. Med. 4 (2023) 101014.
[21] Y. Chen, T. Zhao, M. Bai, et al., Chem. Eng. J. 435 (2022) 135160.
[22] J. Zuo, X. Gao, J. Xiao, et al., Chin. Chem. Lett. 34 (2023) 107827.
[23] X. Zhang, N. Li, S. Zhang, et al., Med. Res. Rev. 40 (2020) 1754–1775.
[24] Y. Ren, L. Mei, C. Huang, et al., ACS Mater. Lett. 5 (2022) 225–234.
[25] A. Song, Y. Wang, J. Xu, et al., Nano Today 54 (2024) 102109.
[26] Y. Du, Y. Guo, X. Xiao, et al., Chem. Eng. J. 442 (2022) 136170.
[27] Y. Ma, X. Zhao, P. Tian, et al., Small 20 (2023) 2306402.